THE EUROPEAN
PHYSICAL JOURNAL PLUS

Check for
updates

Dynamics of spinning test particles around the Kerr–Newman–NUT black hole with quintessence in the Rastall gravity

Farrux Abdulxamidov[1,2,3,a], **Carlos A. Benavides-Gallego**[4,5,b], **Bakhtiyor Narzilloev**[2,6,7,8,c], **Ibrar Hussain**[9,d],
Ahmadjon Abdujabbarov[2,3,10,11,e], **Bobomurat Ahmedov**[2,11,12,f], **Haiguang Xu**[4,5,g]

[1] New Uzbekistan University, Mustaqillik Avenue 54, 100007 Tashkent, Uzbekistan
[2] Ulugh Beg Astronomical Institute, Astronomy St. 33, 100052 Tashkent, Uzbekistan
[3] Institute of Nuclear Physics, Ulugbek 1, 100214 Tashkent, Uzbekistan
[4] School of Physics and Astronomy, Shanghai Jiao Tong University, 800 Dongchuan Road, Minhang, Shanghai 200240, People's Republic of China
[5] Shanghai Frontiers Science Center of Gravitational Wave Detection, 800 Dongchuan Road, Minhang, Shanghai 200240, People's Republic of China
[6] School of Engineering, Central Asian University, 111221 Tashkent, Uzbekistan
[7] Tashkent Institute of Irrigation and Agricultural Mechanization Engineers, Kori Niyoziy, 39, 100000 Tashkent, Uzbekistan
[8] Samarkand State University, University Avenue 15, 140104 Samarkand, Uzbekistan
[9] School of Electrical Engineering and Computer Science, National University of Sciences and Technology, H-12, Islamabad, Pakistan
[10] Tashkent State Technical University, 100095 Tashkent, Uzbekistan
[11] National University of Uzbekistan, 100174 Tashkent, Uzbekistan
[12] Institute of Fundamental and Applied Research, National Research University TIIAME, Kori Niyoziy 39, 100000 Tashkent, Uzbekistan

Abstract This work is devoted to the study of motion of spinning test particles in the spacetime of the Kerr–Newman–NUT black hole with quintessence, in the Rastall gravity theory. We use the so-called Mathisson–Papapetrous–Dixon equation to investigate the dynamics of spinning test particles. We discuss the effect of the particle's spin, s, and the spacetime parameters on the effective potential. Then, we focus on the innermost stable circular orbits (ISCOs) and show the dependence of the ISCO radius on the particle's spin for different values of the metric parameters graphically. Then, we investigate the specific energy and the orbital angular momentum of the particle at the ISCO. Our results show that the black hole's spin parameter a has an evident influence on the ISCO radius, followed by the quintessential parameter, α, the quintessence state parameter, ω, and the Rastall gravity parameter, $\kappa\lambda$. We also discuss the constraint on the particle's spin due to the superluminal bound for co-rotating and counter-rotating orbits, which changes depending on the values of the black hole's parameters. Finally, we compare our results with the results for the Kerr black hole. We found that spacetime parameters increase the ISCO radius for co-rotating and counter-rotating circular orbits. Nevertheless, the energy at the ISCO is not affected strongly by the spacetime parameters for higher values of $|s|$.

1 Introduction

Black holes could be considered laboratories for testing the theories of gravity by analyzing particle motion in their vicinity. The dynamics of massive particles around a black hole horizon could enhance our understanding of the strong gravitational field. The particle motion in the black holes' close vicinity is still considered a successful description of the extreme-mass-ratio-inspiral system. The recent observation of the gravitational waves from the merger of black holes, by LIGO-VIRGO collaboration [1] is based primarily on the theoretical models related to the dynamics of particles in the strong-field regime. Moreover, the images of the supermassive black holes, such as M87* and Sgr A* [2, 3], are the outcomes of the studies of the massless particles motion in the surrounding of black holes. Therefore, it is interesting to explore particle motion in different black hole spacetimes to probe the fundamental Physics in their proximity.

[a] e-mail: farrux@astrin.uz

[b] e-mail: cabenavidesg@sjtu.edu.cn

[c] e-mail: baxtiyor@astrin.uz

[d] e-mail: ibrar.hussain@seecs.nust.edu.pk (corresponding author)

[e] e-mail: ahmadjon@astrin.uz

[f] e-mail: ahmedov@astrin.uz

[g] e-mail: hgxu@sjtu.edu.cn

Springer

It is assumed that the existence of a cosmic fluid around black holes could make the dynamics of particles chaotic in nature. Thus, a better approximation for the motion of stellar compact objects around a supermassive black hole is the dynamics of spinning particles, which is also of astrophysical interest. In the literature, several studies have been conducted to explore the spinning particle motion under the influence of the strong gravitational field of black holes. Test particles with negligible mass and size compared to the central compact object follow geodesics. To consider a more realistic situation, one can incorporate spin in the motion of particles that do not follow geodesic completely and therefore need different types of equations of motion. Mathisson and Papapetrou were the first to present the equations of motion for spinning test particles in gravitational fields [4, 5]. To solve the Mathisson and Papapetrou equations, one needs a spin supplementary condition to overcome the issue of the fewer number of equations than the variables involved there [6]. Dixon then modified the equations of Mathisson and Papapetrou. These equations are known as the Mathisson-Papapetrou-Dixon (MPD) equations of motion in the literature [7]. In the presence of a gravitational field, the dynamics of spinning test particles have been analyzed in the pole-dipole approximation, i.e., by neglecting the effects of the gravitational field and the particle's higher-order multipoles where the particle is assumed to be completely specified by its spin dipole and mass monopole [8]. Using the MPD equations, it has been shown that the orbits are sensitive to the spin-to-mass ratio of the particles in the plan gravitational wave spacetime in the weak field limit [9]. The scattering of spinning test particles in the background of plane gravitational waves and electromagnetic waves have been investigated utilizing the MPD equations [10]. Besides, the dynamics of spinning test particles have been studied in various black hole and wormholes spacetimes, including the Schwarzschild spacetime [11], the Reissner-Nordström spacetime [12], Kerr and Kerr–Newman spacetimes [13, 14], rotating and traversable wormholes [15, 16]. The spinning particles have also been analyzed in theories of gravity other than Einstein's General Relativity (GR), e.g., four-dimensional Einstein-Gauss-Bonnet gravity, where the Gauss-Bonnet parameter has been restricted to a special interval of values depending on the mass of the black hole [17]. In the present work, we are interested in the motion of spinning particles in the spacetime geometry of the Kerr–Newman–NUT–Kiselev (KNNK) black hole in the Rastall theory of gravity (discussed below) [18] to look at the effect of the spacetime parameters on the motion of the spinning particles.

The current accelerated expansion of our observable Universe could be explained with the notion of dark energy [19]. There are several candidates for dark energy, including chaplygin gas, k-essence, the cosmological constant, and quintessence [20]. The range of the equation of state parameter ω for quintessence is defined as $(-1, -1/3)$ and is widely discussed in the cosmological context [21], and also in the context of black hole spacetimes [22]. Kiselev has found a black hole solution of the field equations of GR in the presence of quintessence [22]. Afterward, the Kiselev black hole solution was generalized in the presence of charge and rotating parameters [23]. The Kiselev black hole solution with charge and spin was then derived with the NUT parameter, which has been studied in the literature for particle motion and thermodynamics [24, 25]. The charged-rotating Kiselev black hole solution with the NUT parameter, which is referred as KNNK black hole in the above paragraph here, has also been derived in the Rastall theory of gravity [18]. The motion of massive and measles particles has been analyzed in the vicinity of the KNNK black hole in the Rastall theory of gravity [26–28]. The Joule-Thomson expansion and the optical behaviour of a non-asymptotically flat and charged static black hole spacetime with quintessence, in the Rastall theory of gravity, has also been discussed in the literature [29].

The Brazilian physicist Paulo Rastall [18], proposed a modification of Einstein's theory of GR in the 1970s and introduced the new Rastall gravity parameter. The Rastall modification to GR suggests that the energy-momentum conservation law is not strictly obeyed and that the coupling between the geometry of spacetime and the distribution of matter and energy is modified by the Rastall parameter. The Rastall parameter modifies the Einstein field equations by introducing a non-minimal coupling between the matter and the curvature of spacetime which appears as a new coefficient in the energy-momentum tensor in the gravitational field equations. There are some arguments about the validity of the Rastall theory of gravity. In this regard, Visser has argued that at the large scale, the Rastall theory of gravity is a re-arrangement of the matter sector of the standard GR [30]. Particularly it is argued that on comparison of the GR and Rastall theory of gravity, one may have that the gravity parts of the two theories of gravity are equivalent to each other. A counter-argument has been made where it is shown that the two theories of gravity i.e. the GR and the Rastall theory of gravity are not equivalent and the latter is a modified theory of gravity [31]. The Rastall theory of gravity has then been generalized by taking a modification of the law of conservation of the stress-energy-momentum tensor [32, 33]. Exact solutions in the Rastall theory of gravity have been obtained for static and cylindrically symmetric configurations [34, 35]. Rapidly spinning compact objects have also been studied in the Rastall theory of gravity [36, 37]. In the literature for a suitable choice of the coupling parameter of the Rastall theory of gravity, it has shown that in the presence of the quintessence dark energy parameter, the results in the GR can be recovered [38]. A twisted, charged, and rotating black hole solution with the quintessence dark energy has also been derived in the Rastall theory of gravity [39]. Some other axially symmetric black hole solutions in the Rastall theory of gravity have also been derived in the literature [40, 41]. Investigation of spacetime properties of several black hole solutions through the motion of test particles and photons have been extensively studied in our previous works [28, 42–53].

This paper is organized as follows: In the next section we present the KNNK black hole solution in the Rastall gravity where the horizon structure of the said black hole is also briefly discussed. In Sect. 3, we give the equations of motion for spinning test particles in black hole spacetimes. In the same section, we also give the equations for the effective potential of a test particle in a black hole geometry. In Sect. 4, we analyze the motion of spinning test particles in the vicinity of the KNNK black hole in the Rastall theory of gravity where we also investigate the innermost stable circular orbits (ISCO) of the particles and demonstrate them graphically. In the last section, we give the conclusion of our work.

2 Kerr–Newman–NUT–Kiselev spacetime in the Rastall gravity

GR is a promising theory of gravity, as it has successfully passed observational tests such as the deflection of light by gravitational sources and the generation of gravitational waves from binary black hole systems [1]. Despite our understanding of GR, certain phenomena such as the quantization of gravity on curved backgrounds and the accelerated expansion of the Universe remain unexplained within its framework. As a result, alternative theories of gravity have been proposed [54]. An alternative to GR is the Rastall theory of gravity, in which rotating and non-rotating black hole solutions have been analysed.

The Rastall theory of gravity predicts a specific form for the spacetime metric of the KNNK black hole, found in [39]:

$$ds^2 = -\frac{\Delta}{\Sigma}\{dt - [a\sin^2\theta + 2l(1-\cos\theta)]d\phi\}^2$$
$$+ \frac{\Sigma}{\Delta}dr^2 + \Sigma d\theta^2 + \frac{\sin^2\theta}{\Sigma}\{adt - [r^2 + (a+l)^2]d\phi\}^2, \tag{1}$$

here

$$\Delta = r^2 - 2Mr + a^2 + e^2 + g^2 - l^2 - \alpha r^v, \tag{2}$$

$$v = \frac{1 - 3\omega}{1 - 3\kappa\lambda(1+\omega)}, \tag{3}$$

$$\Sigma = r^2 + (l + a\cos\theta)^2. \tag{4}$$

The KNNK black hole solution in Rastall gravity contains seven parameters. The total mass and the specific angular momentum of the black hole are represented by M and a, respectively. Other parameters include: l, the NUT parameter, α, the quintessential intensity, $\kappa\lambda$, the Rastall gravity parameter, the physical meaning of which has been explored at the large scale [55]. The parameter of the equation of state of the quintessence is denoted by ω, the parameters e and g correspond to the electric and magnetic charges of the black hole, respectively [39]. It is also possible to introduce a new parameter $q^2 = e^2 + g^2$ that takes into account the contribution of both the electric and the magnetic charges of the black hole to the spacetime.

The KNNK black hole solution in Rastall gravity is a unique and interesting solution, as it contains several horizons which depend on the values of the parameters ω and $\kappa\lambda$. The event horizon is a crucial concept in black hole Physics and is determined as the coordinate singularity of the spacetime, which is a null hypersurface of constant r. This means that the event horizon is the surface beyond which the gravitational pull is so strong that nothing, including light, can escape. The horizons in the KNNK black hole solution are determined as the roots of a specific algebraic equation

$$r^2 - 2Mr + a^2 + q^2 - l^2 - \alpha r^v = 0. \tag{5}$$

These equations are used to identify the location of the horizons and study their properties. The presence of multiple horizons in the KNNK black hole solution in Rastall gravity provides a rich and complex structure that is worthy of further investigation.

The number and location of horizons in the KNNK black hole solution in Rastall gravity depend on the values of the parameters ω and $\kappa\lambda$. For certain values of these parameters, the horizon may have only inner and outer parts or may not have a cosmological horizon. These specific cases are of interest as the thermodynamic properties of the black hole are relatively easier to study. This is why in a recent study [56], only two roots of the horizon equation were explored.

However, when the horizon equation has more than two roots, it becomes much more challenging to perform calculations, such as studying the entropy product. A table (given as Table 1, below) of selected values of parameters ω and $\kappa\lambda$ that allow for two analytic roots for the horizon equation can be found in [39].

Table 1 The last column of the table presents the selected values of black hole parameters ω and $\kappa\lambda$ that allow for exact analytical solutions for both the inner and outer horizons

$\omega, \kappa\lambda$	Horizon $(r_\pm)$
0, 0	$\left(M + \frac{\alpha}{2}\right) \pm \sqrt{\left(M + \frac{\alpha}{2}\right)^2 + l^2 - a^2 - q^2}$
$-1/3$, 0	$\frac{M}{1-\alpha} \pm \frac{\sqrt{M^2 - (a^2 + q^2 - l^2)(1-\alpha)}}{1-\alpha}$
0, 1/6	$\frac{M}{1-\alpha} \pm \frac{\sqrt{M^2 - (a^2 + q^2 - l^2)(1-\alpha)}}{1-\alpha}$
$-1/3$, $-1/2$	$\left(M + \frac{\alpha}{2}\right) \pm \sqrt{\left(M + \frac{\alpha}{2}\right)^2 + l^2 - a^2 - q^2}$
1/3, 0	$M \pm \sqrt{M^2 + l^2 + \alpha - a^2 - q^2}$

3 Equation of motion for spinning test particle: basic concepts

In the last section, we discuss the spacetime of a KNNK black hole in the Rastall theory of gravity. Now, to address the motion of spinning test particles in that spacetime, we review the theoretical background necessary to investigate this problem. According to the literature, Mathisson was the first to consider spinning test particle motion while working on extended bodies in GR [4]. Back in 1937, when his work was published, Mathisson showed that spinning test particles do not follow the usual geodesic equation of GR. Instead, spinning test particles follow a differential equation where a coupling between the Riemann curvature tensor and the particle's spin is present. Papapetrou considered a similar approach in Refs. [5, 57] during the 1950s. Then, Tulczyjew and others improved Mathisson's method in Refs. [58–64]. Recently, the MPD equations were modified (see, for example, Refs. [65, 66] and references there in). Nevertheless, in this paper, we stick to the usual MPD equations.

The MPD equations are given by

$$
\frac{Dp^\mu}{d\tau} = -\frac{1}{2} R^\mu_{\ \nu\delta\sigma} u^\nu S^{\delta\sigma},
$$
$$
\frac{DS^{\mu\nu}}{d\tau} = p^\mu u^\nu - p^\nu u^\mu.
$$
(6)

Here, we define the projection of the covariant derivative along the particle's trajectory as $D/d\tau \equiv u^\mu \nabla_\mu$, where $u^\mu = dx^\mu/d\tau$ is the 4-velocity of the test particle, p^μ is the canonical 4-momentum, $R^\mu_{\ \nu\delta\sigma}$ is the Riemann curvature tensor, and τ is an affine parameter. It is important to remark that the second rank tensor $S^{\mu\nu}$ in the Eq. (6) is antisymmetric. Therefore, $S^{\mu\nu} = -S^{\nu\mu}$.

On the other hand, as mentioned above, the motion of spinning test particles is described by differential equations coupled with the Riemann curvature tensor; see the first relation in Eq. (6). When the components of $S^{\mu\nu}$ vanish, the differential equation reduces to

$$
\frac{Dp^\mu}{d\tau} = 0,
$$
(7)

corresponding to the well-known geodesic equation of GR when one expresses it in terms of the 4-momentum and the projection of the covariant derivative along the particle's trajectory.

To solve the set of equations (6), one needs to fix the center of mass. In this sense, it is necessary to consider the Tulczyjew Spin Supplementary Condition (SSC) [67], given by the relation [58, 67]

$$
S^{\mu\nu} p_\mu = 0,
$$
(8)

from which, the canonical momentum and the spin of the particle provide two independent conserved quantities, given by the relations:

$$
S^{\mu\nu} S_{\mu\nu} = 2S^2,
$$
$$
p^\mu p_\mu = -m^2.
$$
(9)

In addition to the spin and the canonical momentum shown in Eq. (9), one also has the usual conserved quantities associated with the spacetime symmetries. In the case of an axially symmetric spacetime, there are two Killing vectors field. One is related to invariant time translations, ξ^μ, and the other generates rotations along the azimuth angle ϕ, ψ^μ. We can compute these quantities using the following equation:

$$
p^\mu \kappa_\mu - \frac{1}{2} S^{\mu\nu} \nabla_\nu \kappa_\mu = p^\mu \kappa_\mu - \frac{1}{2} S^{\mu\nu} \partial_\nu \kappa_\mu = \text{constant},
$$
(10)

where k^μ is one of the two Killing vector fields; i.e., ξ^μ or ψ^μ.

Finally, in contrast to the conservation of canonical momentum [see the second relation in Eq. (9)], it is crucial to mention that for the spinning test particles the four velocity is a timelike unit vector:

$$
u_\mu u^\mu \neq -1.
$$
(11)

The reason for such behavior has to do with the fact that p^μ and u^μ are not always parallel. From the physical point of view, the violation of Eq. (11) enables spinning test particles to move faster than the speed of light, something forbidden by physical laws. In this sense, to avoid this problem, it is necessary to impose an additional condition the *superluminal bound* as mentioned in [68].

The superluminal bound is an important condition for the dynamics of spinning test particles. This constraint will help us to find the values of s for which the particle's trajectory is time-like. As we remarked before, although $p_\mu p^\mu = -m^2$ holds, the normalization $u_\mu u^\mu = -1$ is not necessarily satisfied. Therefore, the four-velocity u^μ increases, and for specific values of spin s, some of the u^μ components may diverge. Hence, the particle's trajectory becomes space-like and without physical meaning.

In order to maintain the trajectory of spinning test particles with time-like character, it is necessary to impose the following constraint (on the equatorial plane) [68–71]

$$
\frac{u_\mu u^\mu}{(u^t)^2} = g_{tt} + g_{rr} \left(\frac{dr}{dt}\right)^2 + 2g_{t\varphi} \frac{d\varphi}{dt} + g_{\varphi\varphi} \left(\frac{d\varphi}{dt}\right)^2 \leq 0.
$$
(12)

Hence, by solving the MPD equations (6), one obtains the following general expressions for dr/dt and $d\phi/dt$ [68, 69, 72]

$$\frac{dr}{dt} = \frac{u^r}{u^t} = \frac{\mathcal{C}p_r}{\mathcal{B}p_t + \mathcal{D}p_\varphi},$$
$$\frac{d\varphi}{dt} = \frac{u^\varphi}{u^t} = \frac{\mathcal{D}p_t + \mathcal{A}p_\varphi}{\mathcal{B}p_t + \mathcal{D}p_\varphi}. \tag{13}$$

where

$$\mathcal{A} = g^{\varphi\varphi} + \left(\frac{S^{\varphi r}}{p_t}\right)^2 R_{trrt},$$

$$\mathcal{B} = g^{tt} + \left(\frac{S^{\varphi r}}{p_t}\right)^2 R_{\varphi rr\varphi},$$

$$\mathcal{C} = g^{rr} + \left(\frac{S^{\varphi r}}{p_t}\right)^2 R_{\varphi tt\varphi}, \tag{14}$$

$$\mathcal{D} = g^{t\varphi} + \left(\frac{S^{\varphi r}}{p_t}\right)^2 R_{tr\varphi r}.$$

In this sense, by defining the function $\mathcal{F} = u_\mu u^/(u^t)^2$, one obtains the value of s for which $\mathcal{F} = 0$, the superluminal bound. Therefore, when $\mathcal{F} > 0$ for a certain value of s, the trajectory of the spinning test particle is space-like, and s is a forbidden value. If $\mathcal{F} < 0$, the particle's trajectory is time-like, and the corresponding value of s is allowed.

3.1 The effective potential

The motion of spinning test particles can be analyzed using the effective potential, V_{eff}, a function relating the energy, E, the total angular momentum J, and the particle's spin, s. In particular, we can investigate the dynamics of spinning test particles when they follow stable circular orbits, finding in this way, through the superluminal bound, a constraint on s.

In the case of static and axially symmetric spacetimes,

$$ds^2 = g_{tt}dt^2 + g_{rr}dr^2 + 2g_{t\varphi}dtd\phi + g_{\theta\theta}d\theta^2 + g_{\phi\phi}d\phi^2, \tag{15}$$

the conserved quantities E and J are given by the relations [see Eq. (10)] [69]

$$-E = p_t - \frac{1}{2}\left(g'_{tt}p_\phi - g'_{\phi t}p_t\right)\frac{S^{tr}}{p_\phi}$$

$$J = p_\phi - \frac{1}{2}\left(g'_{t\phi}p_\phi - g'_{\phi\phi}p_t\right)\frac{S^{tr}}{p_\phi}, \tag{16}$$

where the motion is assumed to be constrained to the equatorial plane, $\theta = \pi/2$, and $'$ denotes the radial derivative. Moreover, since the particle's motion is constrained to the equatorial plane, the antisymmetric tensor $S^{\mu\nu}$ only has three independent components, i. e. [68, 69, 71],

$$S^{t\phi} = \frac{p_r}{p_t}S^{\phi r} = -\frac{p_r}{p_\phi}S^{tr},$$

$$S^{r\varphi} = -\frac{p_t}{p_\varphi}S^{rt} = \frac{p_t}{p_\varphi}S^{tr}. \tag{17}$$

See Eq. (8). Therefore, the energy, E, and the total angular momentum, J, reduce to Eq. (16). On the other hand, from the spin conservation and the normalization conditions, Eqs. (9), we have that

$$S^{tr} = \frac{p_\phi s}{\sqrt{g_{rr}(g_{t\phi}^2 - g_{\phi\phi}g_{tt})}}. \tag{18}$$

Here, $s = S/m$ represents the specific angular momentum of the particle (spin), which can be positive or negative depending on the direction of p_φ. After replacing Eq. (18) into Eq. (16) and solving the system for p_t and p_ϕ, we obtain [68, 69]

$$p_t = \frac{-E + s(AJ + BE)}{1 - Ds^2}$$

$$p_\phi = \frac{J + s(BJ + CE)}{1 - Ds^2}, \tag{19}$$

Fig. 1 The radial dependence of the effective potential for different values of the spin of the particle while keeping all other parameters constant
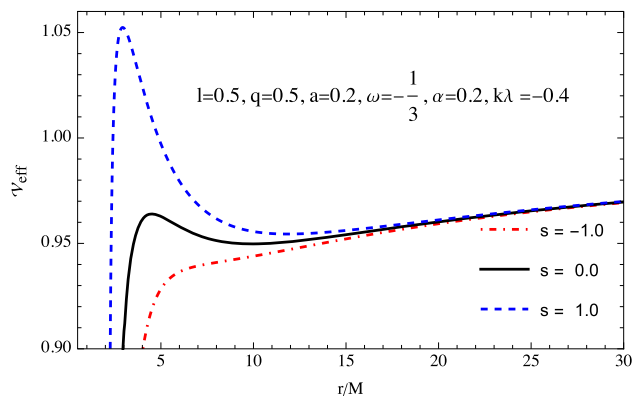
with

$$A = \frac{g'_{tt}}{2\sqrt{g_{rr}(g_{t\phi}^2 - g_{\phi\phi}g_{tt})}},$$

$$B = \frac{g'_{t\phi}}{2\sqrt{g_{rr}(g_{t\phi}^2 - g_{\phi\varphi}g_{tt})}},$$

$$C = \frac{g'_{\phi\phi}}{2\sqrt{g_{rr}(g_{t\phi}^2 - g_{\phi\varphi}g_{tt})}},$$

$$D = \frac{(g'_{t\phi})^2 - g'_{tt}g'_{\phi\phi}}{4g_{rr}(g_{t\phi}^2 - g_{\phi\phi}g_{tt})}. \tag{20}$$

Now, from Eqs. (9) and (19), the radial canonical momentum is given by

$$p_r^2 = \frac{\beta}{\alpha}\left(E^2 + \frac{\delta J}{\beta}E + \frac{\sigma J^2}{\beta} - \frac{\rho}{\beta}\right). \tag{21}$$

The last expression can be written in the following way:

$$p_r^2 = \frac{\beta}{\alpha}(E - V_{\text{eff}}^+)(E - V_{\text{eff}}^-), \tag{22}$$

from which

$$V_{\text{eff}}^{\pm} = \frac{-\delta J \pm \sqrt{(\delta J)^2 - 4\gamma\beta}}{2\beta}, \tag{23}$$

where $\gamma = \sigma J^2 - \rho$. The general expressions for $\alpha, \beta, \delta, \sigma$ and ρ in the case of a static and axially symmetric spacetime are given in Eq. (36) of the Ref. [69].

In Sect. 4, we will apply Eq. (23) to the KNNK black hole in the Rastall Gravity. To perform our analysis, we use the dimensionless variables $\mathcal{J}, \mathcal{E}, s$. These variables are defined as

$$\mathcal{E} \to \frac{E}{m}, \quad \mathcal{J} \to \frac{\mathcal{J}}{M} = \frac{J}{mM}, \quad s \to \frac{s}{M} = \frac{S}{mM}. \tag{24}$$

Here m the mass of the spinning test particle. Hence, the effective potential reduces to

$$\mathcal{V}_{\text{eff}}^{\pm} \to \frac{V_{\text{eff}}^{\pm}}{m} = \frac{-\delta \mathcal{J} \pm \sqrt{(\delta \mathcal{J})^2 - 4\gamma\beta}}{2\beta}. \tag{25}$$

In the case of the spin of the black hole, a, the dimensionless variable is defined as $a \to a/M^2$. And the dimensionless radial coordinate is given by $r \to r/M$.

From now on, we constrain our attention to the case of test particles with positive energy, in this sense, $\mathcal{V}_{\text{eff}} \equiv \mathcal{V}_{\text{eff}}^+$.

4 Dynamics of spinning test particles around Kerr–Newman–NUT–Kiselev black holes in the Rastall gravity

In this section, we apply the results of Sect. 3 to the particular case of KNNK black holes in the Rastall gravity. First, we investigate the effects of the spacetime parameters: $a, \alpha, \omega,$ and $\kappa\lambda$ on the effective potential. Then we focus on the discussion about the stable
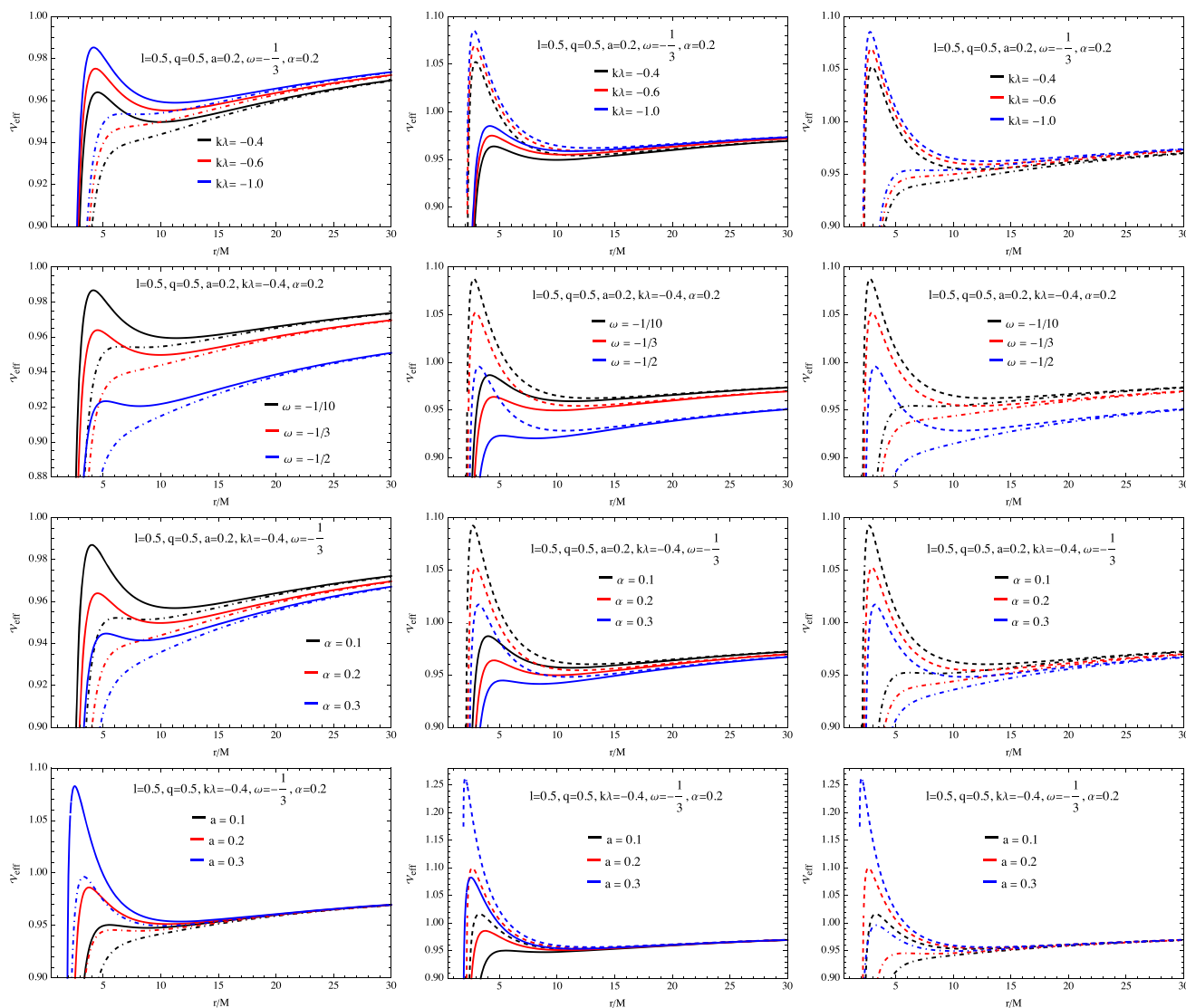
Fig. 2 The radial dependence of the effective potential. Here the dot-dashed, solid, and dashes lines represent the case of a spinning test particle with $s = -1$, $s = 0$, and $s = 1$, respectively. In all plots, the particle's orbital angular momentum is $\mathcal{L} = 5$

circular orbits. Here, we also discuss the effect of the spacetime parameters on $\mathcal{L}$ and $\mathcal{E}$. Finally, we discuss the superluminal bound, which allows us to constrain the possible values of the particle's spin, s, in the KNNK spacetime in the Rastall gravity.

4.1 The effective potential

Using the metric (1) and the results of Sect. 3, we obtain the analytical expression for $\mathcal{V}_{\mathrm{eff}}$ of the spinning test particle in the field of the KNNK black hoe in the Rastall gravity, see Eq. (25). Nevertheless, the explicit form of the effective potential involving δ, γ, and β is long enough to be included in the manuscript. Instead, we prefer the use of figures to demonstrate the effects of the spacetime parameters on $\mathcal{V}_{\mathrm{eff}}$.

Figures 1 and 2 shows dependence of the effective potential on the radial coordinate for spinning test particles in the KNNK black hole spacetime in the Rastall gravity. Since we consider several parameters, we keep constant the NUT parameter, $l = 0.5$, and the parameter $q = 0.5$, focusing only on the quintessential intensity, α, the Rastall gravity parameter, $\kappa\lambda$, and the quintessence state parameter, ω. In the Fig. 2, we use dot-dashed, solid, and dashed lines to depict $\mathcal{V}_{\mathrm{eff}}$ of test particles with spin, $s = -1$, $s = 0$, and $s = 1$, respectively. Note that the first column of Fig. 2 compares the potential of a spinning test particle with $s < 0$ and that of a test particle without spin, while the second column compares $\mathcal{V}_{\mathrm{eff}}$ for $s > 0$ and $s = 0$. In the third column, we contrast the potential for test particles with negative and positive spins.

Fig. 3 Dependence of the ISCO radius on the spin of the particle for the different values of the spacetime parameters (Left side plots for co-rotating case, right side for counter-rotating)
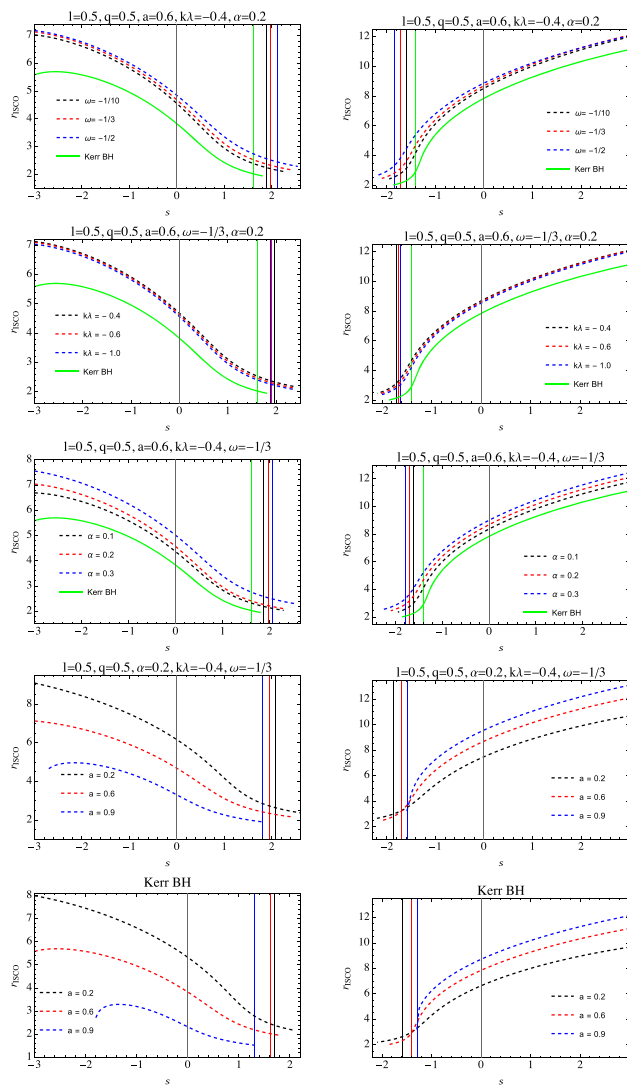
In all the figures, the effective potential behaves as usual: it tends to $\mathcal{V}_{\text{eff}} = 1$ when $r/M \to \infty$ and diverges when the radial coordinate tends to the horizon. Furthermore, $\mathcal{V}_{\text{eff}}$ has a maximum value, which is more evident for particles with $s = 0$ and $s = 1$. We obtain a similar conclusion in the case of the minimum value of the effective potential.

Our objective is to examine the impact of the spin of the particle while maintaining constant values for all other parameters. Figure 1 demonstrates that the effective potential rises with an increase in particle's spin. Moreover, note that values of $\mathcal{V}_{\text{eff}}$ are bigger when the test particle's spin is positive, and smaller when the particle's spin is negative. On the other hand, according to Fig. 2, as the $k\lambda$ parameter increases, it results in a decrease in the effective potential. While we see opposite behavior, if we consider different values of the black hole's angular momentum, a, see the fourth row in Fig. 2. In the second row of Fig. 2, we plot the behavior of $\mathcal{V}_{\text{eff}}$ as a function of r/M for different values of the quintessence state parameter, ω. In all the three cases ($s = -1$, $s = 0$, and $s = 1$), the figure shows that $\mathcal{V}_{\text{eff}}$ decreases as ω changes from $-1/10$ to $-1/2$.

Finally, in the third row of Fig. 2, we show the behavior of $\mathcal{V}_{\text{eff}}$ for different values of the quintessential intensity, α. From the figure, it is possible to see that the potential reduces as α increases independently of the sign of the particle's spin.

4.2 Innermost stable circular orbit

Now we study the circular orbits of spinning test particles in the spacetime of KNNK black hole in the Rastall gravity, governed by the metric Eq. (1). It is well-known that particles travel in circular orbits when the following conditions are hold simultaneously: (a) zero radial velocity ($dr/d\tau = 0$) and (b) zero radial acceleration ($d^2r/d\tau^2 = 0$), or equivalently, $\mathcal{E} = \mathcal{V}_{\text{eff}}$ and $d\mathcal{V}_{\text{eff}}/dr = 0$.

Fig. 4 Dependence of the angular momentum at the ISCO radius on the spin of the particle for the different values of the spacetime parameters (Left side plots for co-rotating case, right side for counter-rotating)
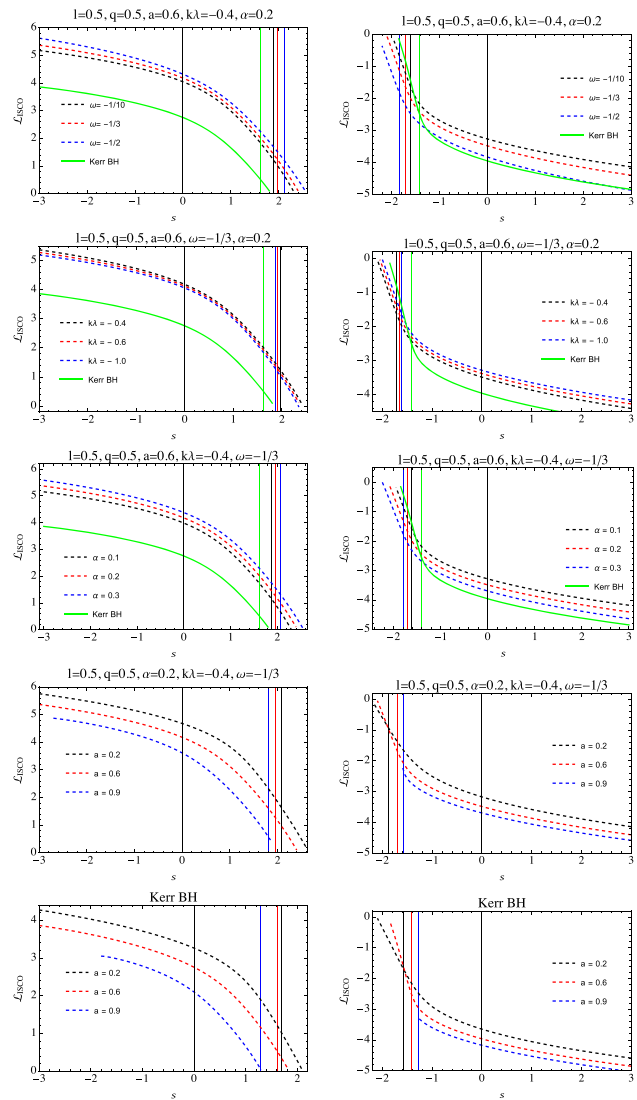
Nevertheless, these conditions do not guarantee the stability of the circular orbit. Therefore, it is necessary to impose an additional constraint on $\mathcal{V}_{\text{eff}}$, that is:

$$\frac{d^2\mathcal{V}_{\text{eff}}}{dr^2} \geq 0. \tag{26}$$

In the last equation, the innermost region of the stable circular orbits is obtained when the equality condition in Eq. (26) holds. This region is known as the ISCO. To obtain the radius of the ISCO, the total angular momentum, $\mathcal{J}_{\text{ISCO}}$, and the energy per unit mass, $\mathcal{E}_{\text{ISCO}}$, we solve numerically and simultaneously the non-linear system $d\mathcal{V}_{\text{eff}}/dr = 0$ and $d^2\mathcal{V}_{\text{eff}}/dr^2 = 0$ for r_{ISCO} and $\mathcal{J}_{\text{ISCO}}$. Then, with the help of Eq. (25) we compute the value of $\mathcal{E}_{\text{ISCO}}$.

In Figs. 3, 4, 5, 6 and 7, we plot the behavior of r_{ISCO}, $\mathcal{L}_{\text{ISCO}}$, $\mathcal{E}_{\text{ISCO}}$ as a function of s for different values of the metric parameters a, α, ω, and $\kappa\lambda$. It is important to mention that in all the figures, the left and right columns correspond to co-rotating ($\mathcal{L}_{\text{ISCO}} > 0$) and counter-rotating ($\mathcal{L}_{\text{ISCO}} < 0$) orbits, respectively. Note that we are considering only the particle's orbital angular moment, $\mathcal{L}_{\text{ISCO}}$, instead of its total angular momentum, $\mathcal{J}_{\text{ISCO}}$, related to the former by the relation $\mathcal{J}_{\text{ISCO}} = \mathcal{L}_{\text{ISCO}} + s$. This is done to define the co-rotating and counter-rotating orbits in the usual way.

In Fig. 3, we show the dependence of the r_{ISCO} on the spin of the particle, s, for the different values of the spacetime parameters, $\omega, \kappa\lambda, \alpha$, and a. Note that the left and right panels correspond to co-rotating and counter-rotating orbits, respectively. In the same figure, when one consider different values of the quintessence state parameter, ω, it is possible to see that r_{ISCO} decreases as ω increases for a constant value of the particle's spin. This behavior is the same for the co-rotating and counter-rotating orbits; see the first row in Fig. 3. Furthermore, for constant values of ω, the figure shows the ISCO radius for cor-rotating orbits decreases when the particle's spin increases in contrast to counter-rotating orbits, where r_{ISCO} increases as s increases.

Fig. 5 Dependence of the specific energy at the ISCO radius on the spin of the particle for the different values of the spacetime parameters (Left side plots for co-rotating case, right side for counter-rotating)
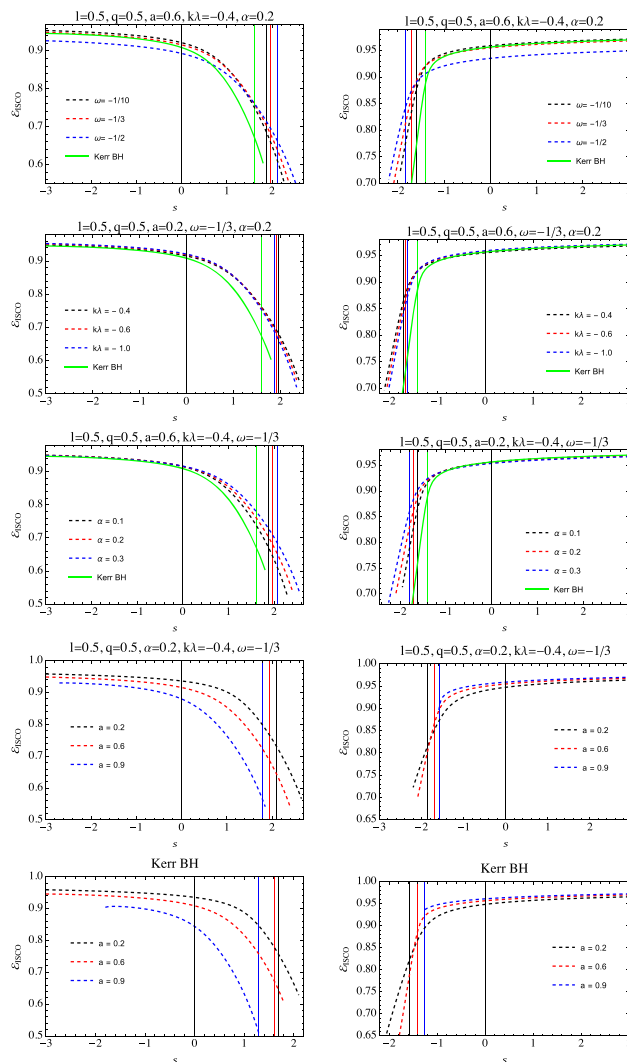

In the second row of Fig. 3, we show the behavior of r_{ISCO} as a function of s for different values of the Rastall gravity parameter, $\kappa\lambda$. Similar to the previous case, the ISCO radius (when $\kappa\lambda$ is constant) decreases/increases as the spin s increases for co-rotating/counter-rotating orbits. Note this trait is common in all situations where their corresponding metric parameters are constant, i.e., when ω, $k\lambda$, α, a are constants. On the other hand, for both co-rotating and counter-rotating orbits, when $\kappa\lambda$ decreases from -0.4 to -1 (while keeping constant the particle's spin), r_{ISCO} reduces its value.

In the third row of Fig. 3, we plot r_{ISCO} versus s for different values of α, the quintessential intensity. From the figure, it is possible to see how the ISCO radius decreases as the α parameter changes from 0.1 to 0.3 when co-rotating and counter-rotating orbits have a constant value of s. Note how the changes in r_{ISCO} are more evident when α varies than the cases in which ω and $\kappa\lambda$ change, see the first and second rows in the figure. Nevertheless, this variation is less evident when compared with that in which the black hole's spin, a, increases from 0.2 to 0.9. See the last row in Fig. 3.

The behavior of r_{ISCO} versus s for different values of the black hole's spin, a, is shown in the fourth row of Fig. 3. For constant values of the particle's spin, the figure shows how the ISCO radius of co-rotating orbits increases as the black hole's spin decreases from 0.9 to 0.2. Nevertheless, the opposite behavior occurs when the spinning test particle follows a counter-rotating circular orbit: the ISCO radius decreases as a increases. Furthermore, note that the difference in the values of ISCO is more evident than the other spacetime parameters when the black hole's spin varies.

In the figure Fig. 3, we also show the behavior of r_{ISCO} in the Kerr spacetime; see the continuous green line in the first, second, and third rows, and the panels in the fifth rows of Fig. 3. The effect of ω, $\kappa\lambda$, and α is evident: r_{ISCO} increase its value in the presence of the metric parameters, which means that spinning test particles move farther from the KNNK black hole's center in contrast to the Kerr black hole. We see that the effect of a on r_{ISCO} is quite similar in both cases. We plot them in different figures to compare; see the panels in the fourth and fifth rows in Fig. 3.

Fig. 6 Dependence of the specific energy on the ISCO radius of the particle for the different values of the spacetime parameters (Left side plots for co-rotating case, right side for counter-rotating)
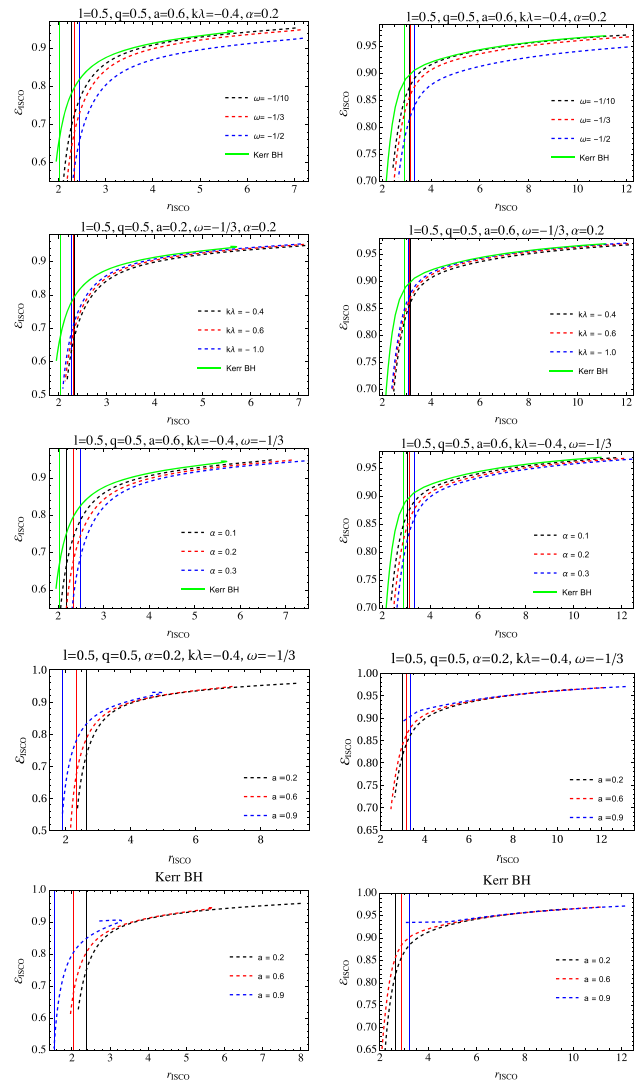

On the other hand, as discussed in Sect. 3, to keep the trajectory of spinning test particles time-like, it is necessary to impose the superluminal bound, defined by the function $\mathcal{F}$ through Eq. (12). From the physical point of view, the superluminal bound corresponds to the value of s for which the function $\mathcal{F} = 0$. In this sense, circular orbits with $s \leq s_{\text{luminal}}$ are time-like, and therefore, physically allowed ($\mathcal{F} \leq 0$). In the Fig. 3, vertical lines depict the superluminal bond ($s = s_{\text{luminal}}$). According to the figure Fig. 3, when we consider different values of ω, the superluminal bound for co-rotating circular orbits increases as ω changes from $-1/10$ to $-1/2$; nevertheless, in the case of counter-rotating spinning test particles, s_{luminal} reduces its value. Therefore, particles following co-rotating circular orbits have a larger range of allowed orbits than counter-rotating particles. A similar behavior occurs when the parameter α changes from 0.1 to 0.3. However, the variation in s_{luminal} is more symmetric than the previous case (first row); see the third row in Fig. 3.

When we consider different values of $\kappa\lambda$, the second row of Fig. 3 shows that s_{luminal} increases/decreases as $|\kappa\lambda|$ reduces its value from 1 to 0.4 for co-/counter-rotating circular orbits. Moreover, note that s_{luminal} does not change considerably in this case when contrasted with the other parameters. We obtain the same behavior for different values of a; see the fourth row of Fig. 3. Note that the changes in s_{luminal} are the most notorious and symmetric of all cases. In the same figure, we also show the ISCO for the Kerr black hole for different values of a. See the last row of the same figure. Although s_{luminal} also increases/decreases as a decreases for co-/counter-rotating orbits in the Kerr black hole, it is possible to see that the change is not symmetric when compared to the KNNK black hole.

Figure 4 illustrates the behavior of $\mathcal{L}_{\text{ISCO}}$ versus s for different values of the metric parameters. According to the first row in the Fig. 4, it is clear that an increment of s decreases the spinning test particle's angular momentum in both co- and counter-rotating cases. Moreover, for a constant value of s, note that reducing the value of the parameter ω increases the value of $\mathcal{L}_{\text{ISCO}}$ for co-rotating orbits; in contrast to the counter-rotating case, where the particle's angular momentum reduces its value.

Fig. 7 Dependence of the specific energy on the angular momentum at the ISCO radius of the particle for the different values of the spacetime parameters (Left side plots for co-rotating case, right side for counter-rotating)
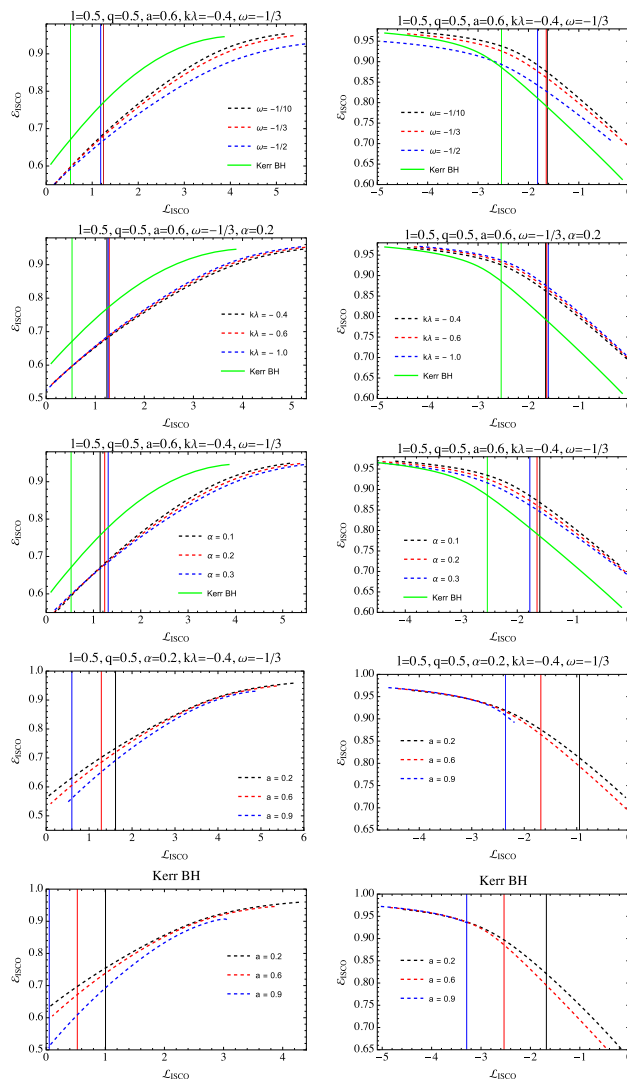
The second row of Fig. 4 describes the effect of the Rastall gravity parameter, $\kappa\lambda$, in the $\mathcal{L}_{ISCO}$. In the case of co-rotating circular orbits, the same figure shows that decreasing the values of the Rastall parameter decreases the spinning test particle's angular momentum slightly, while its value increases when the spinning test particle follows a counter-rotating orbit.

In the third row of Fig. 4, we plot the angular momentum as a function of s for different values of α. It can be seen how $\mathcal{L}_{ISCO}$ increases for larger values of the quintessential intensity in the case of co-rotating but decreases for the counter-rotating case.

The fourth row of Fig. 4, on the other hand, illustrates the effect of the black hole's spin, a, on $\mathcal{L}_{ISCO}$ against the spin of the test particle. This figure shows clearly that co- and counter-rotating cases are asymmetric, in contrast to previous considerations; see the left and right panels. Moreover, similar to r_{ISCO}, the dependence of $\mathcal{L}_{ISCO}$ on a is much stronger when compared with the other parameters.

The behavior of $\mathcal{L}_{ISCO}$ is depicted in the last row of the figure for the Kerr black hole. Once again, note that the values of $\mathcal{L}_{ISCO}$ in the Kerr black hole are smaller than those in the KNNK black hole for both co-rotating and counter-rotating orbits. Moreover, when we consider the superluminal bound, $s_{luminal}$, we can see that it decreases/increases its value for co-rotating/counter-rotating orbits when compared with the KNNK black hole.

Figure 5 gives us the comportment of the specific energy, $\mathcal{E}_{ISCO}$, as a function of s for different values of ω, $\kappa\lambda$, α, and a. Note the general tendency of co-rotating/counter-rotating orbits is to decrease/increase the specific energy when the particle's spin increases. The first row shows that the bigger the values of ω, the bigger the specific energy in both co-and counter-rotating cases. This behavior continues until some specific value of the test particle's spin. These values correspond to the joining point of the lines around $s \approx +1.5/-1.6$ for co-/counter-rotating cases. The second row of the same figure shows the behavior for different values of the Rastall parameter, $\kappa\lambda$. From the Fig. 5, one can see again the weak effect of this parameter, which negligibly increases the specific energy for smaller negative values of $\kappa\lambda$ in both co- and counter-rotating cases.

On the other hand, the effect of quintessential intensity, α, shown in the third row of Fig. 5, is noticeable only in the neighborhood of the superluminal bound; i.e., $1 < s < 2/ -2 < s < -1$ for co-/counter-rotating cases. Note that all panels of Fig. 5 beside the ones in the fourth and fifth rows are symmetric when the spin transforms as $s \rightarrow -s$. Moreover, according to the fourth row of the same figure, the left panel reveals that increasing the value of a shifts the particle's specific energy downward considerably for co-rotating orbits while shifting the lines upward slightly in the counter-rotating case. The Kerr black hole experiences the same behavior with similar values. Nevertheless, note that the superluminal bound changes considerably (especially for co-rotating orbits) when ω, $\kappa\lambda$, and α vanish. See the fifth row in the figure Fig. 5.

In Fig. 6, we present the dependence of the specific energy on the corresponding ISCO radius of the spinning test particle for different values of the spacetime parameters. The Fig. 6 shows that co- and counter-rotating cases have the same behavior, except for the panels in the fourth row, where we depict the behavior of $\mathcal{E}_{\mathrm{ISCO}}$ for different values of a. Moreover, note that $\mathcal{E}_{\mathrm{ISCO}}$ in the case of Kerr black hole (the continuous green line) is bigger in all the cases, especially in the neighborhood of the superluminal bound.

In the first row, when ω changes from $-1/2$ to $-1/10$, the panels in Fig. 6 show that the lines are shifted upward, increasing the energy of the test particle at the ISCO. Nevertheless, when we consider the Rastall parameter, it can be produce a negligible effect on $\mathcal{E}_{\mathrm{ISCO}}$ since the variations of $\kappa\lambda$ slightly increase its value. Moreover, the panels in the third row of Fig. 6 show that the quintessential intensity parameter has a weak influence on $\mathcal{E}_{\mathrm{ISCO}}$ for higher values of the r_{ISCO}; i.e., far from the central black hole and its influence near the black hole becomes considerable. It clearly shows that higher values of α force the particle to orbit a smaller ISCO, decreasing its specific energy.

Finally, we illustrate the effect of KNNK the black hole's spin, a, on the spinning test particle's energy in the last row of Fig. 6. Note that far from the black hole's center, the effect of a is negligible. However, at closer distances, the increment of this parameter increases the specific energy. The same behavior occurs for the Kerr black hole, see the last row in the figure Fig. 6.

Figure 7 demonstrates the relation between the specific energy of the spinning test particle and its orbital angular momentum for different values of the spacetime parameters of the KNNK black hole in the Rastall gravity. This time, there is no trait of symmetrical behavior between co- and counter-rotating cases, i.e., when $s \rightarrow -s$. Moreover, note that $\mathcal{E}_{\mathrm{ISCO}}$ in the Kerr black hole (continuous green line) tends to have higher/smaller values for co- and counter-rotating orbits.

In the first row of Fig. 7, we can see that higher values of ω require the spinning test particle to move in a circular orbit with higher energy for both co- and counter-rotating cases (when we fix the orbital angular momentum). On the other hand, the effect of the Rastall parameter on $\mathcal{E}_{\mathrm{ISCO}}$ is small for co-rotating orbits, in contrast to the counter-rotating case, where the effect is a bit more evident. In both cases, greater values of the Rastall parameter, $\kappa\lambda$, decrease the energy for a constant $\mathcal{L}_{\mathrm{ISCO}}$. See the second row of Fig. 7.

The third row of Fig. 7 provides the behavior of $\mathcal{E}_{\mathrm{ISCO}}$ versus $\mathcal{L}_{\mathrm{ISCO}}$ for different values of the quintessential intensity. In both cases (co- and counter-rotating orbits), while keeping constant the orbital angular momentum, the value of the specific energy increases when α goes from 0.3 to 0.1.

Lastly, in the fourth row of Fig. 7, we show the effect of the rotation parameter on $\mathcal{E}_{\mathrm{ISCO}}$. According to these panels, the impact of a on the energy is evident for smaller values of $|\mathcal{L}_{\mathrm{ISCO}}|$ and becomes negligible when it increases. One can also note that the faster a black hole spins, the smaller the specific energy of the spinning test particle for a fixed value of its orbital angular momentum. The Kerr black hole experiences similar behavior with different values, especially when $0 < \mathcal{L}_{\mathrm{ISCO}} < 1.5$ and $-3 < \mathcal{L}_{\mathrm{ISCO}} < -1$, for co-rotating and counter-rotating orbits respectively.

5 Conclusion

In this manuscript, we have studied the dynamics of spinning test particles around Kerr–Newman–NUT black hole with quintessence in the Rastall gravity. We have based our analysis on the well-known MPD equations, from which we have obtained the effective potential in terms of the particle's spin, s, and the metric parameters, i.e., the quintessence state parameter, ω, the Rastall gravity parameter, $\kappa\lambda$, the quintessential intensity, α, and the black hole's spin, a, keeping constant the value of the NUT parameter, l, and the parameter q, related to the electric and magnetic charges.

Our results show that the spinning test particle's effective potential increases when its spin increases. Moreover, $\mathcal{V}_{\mathrm{eff}}$ also increases its value when the equation-of-state parameter and the black hole's spin increase. However, when the Rastall parameter and the quintessential intensity increase, the results show the opposite behavior i.e. the particle's effective potential reduces its value. It is worth mentioning that at large distances all the parameters except the black hole's spin, a, influence the particle's effective potential. Nevertheless, closer to the black hole, the parameter a dominates.

The presence of the metric parameters ω, $\kappa\lambda$, α, and a have an evident effect on ISCO radius when compared with the Kerr black hole. The result shows that ISCO radius increases its value for both the co-rotating and counter-rotating orbits, which means that spinning test particles move farther from the black hole center in the KNNK black hole in the Rastall gravity than in the Kerr black hole spacetime of GR. Moreover, when contrasting the effect between the metric parameters, we have found that the Rastall gravity parameter, $\kappa\lambda$, has the lowest impact on ISCO radius, followed by the quintessence state parameter, ω, the quintessential intensity, α, and the black hole's spin, a. The latter having the highest repercussion of all the cases considered in this work, especially for co-rotating circular orbits.

We have noticed that the superluminal bound is also affected by the presence of the metric parameters. In the case of co-rotating circular orbits, for example, the value of $s_{luminal}$ is always higher than that of the Kerr black hole, in the case of counter-rotating orbits. Our analysis show that $\kappa\lambda$ has the lowest impact on $s$luminal, while the black hole's spin parameter, a, has the most evident repercussion on the values of $s_{luminal}$. Hence, co-rotating orbits have an ampler range of stable circular orbits than the counter-rotating ones.

It is worth noticing that co-rotating particles move closer to the black hole's center with $|\mathcal{L}_{ISCO}|$ higher than particles in counter-rotating orbits. Particles moving at the ISCO and following a co-rotating circular orbit need less energy and can spin faster. Particles in a counter-rotating orbit, on the other hand, require more energy if they spin faster.

Data Availability Statement This manuscript has no associated data. (There is no observational data related to this article.)

References

1. B.P. Abbott, R. Abbott, T.D. Abbott, M.R. Abernathy, F. Acernese, (LIGO Scientific Collaboration and Virgo Collaboration), Phys. Rev. Lett. **116**, 061102 (2016). https://doi.org/10.1103/PhysRevLett.116.061102
2. K. Akiyama et al., (Event Horizon Telescope), Astrophys. J. Lett. **875**, L1 (2019). https://doi.org/10.3847/2041-8213/ab0ec7. arXiv:1906.11238 [astro-ph.GA]
3. K. Akiyama et al., (Event Horizon Telescope), Astrophys. J. Lett. **930**, L12 (2022). https://doi.org/10.3847/2041-8213/ac6674
4. M. Mathisson, Gen. Relativ. Gravit. **42**, 1011 (2010)
5. A. Papapetrou, Proc. R. Soc. Lond. Ser. A. Math. Phys. Sci. **209**, 248 (1951)
6. G. Lukes-Gerakopoulos, Phys. Rev. D **96**, 104023 (2017). https://doi.org/10.1103/PhysRevD.96.104023
7. W.G. Dixon, Proc. R. Soc. Lond. A. Math. Phys. Sci. **314**, 499 (1970)
8. M. Zhang, J. Jiang, Phys. Lett. B **834**, 137476 (2022). https://doi.org/10.1016/j.physletb.2022.137476
9. M. Mohseni, H.R. Sepangi, Class. Quantum Gravity **17**, 4615 (2000). https://doi.org/10.1088/0264-9381/17/22/302
10. S. Kessari, D. Singh, R.W. Tucker, C. Wang, Class. Quantum Gravity **19**, 4943 (2002). https://doi.org/10.1088/0264-9381/19/19/312
11. P.I. Jefremov, O.Y. Tsupko, G.S. Bisnovatyi-Kogan, Phys. Rev. D **91**, 124030 (2015). https://doi.org/10.1103/PhysRevD.91.124030
12. D. Bini, G. Gemelli, R. Ruffini, Phys. Rev. D **61**, 064013 (2000). https://doi.org/10.1103/PhysRevD.61.064013
13. O. Semerák, T. Zellerin, M. Žáček, Mon. Not. R. Astron. Soc. **308**, 691 (1999). https://doi.org/10.1046/j.1365-8711.1999.02748.x
14. Y.-P. Zhang, S.-W. Wei, W.-D. Guo, T.-T. Sui, Y.-X. Liu, Phys. Rev. D **97**, 84056 (2018). https://doi.org/10.1103/PhysRevD.97.084056
15. F. Abdulxamidov, C.A. Benavides-Gallego, W.-B. Han, J. Rayimbaev, A. Abdujabbarov, Phys. Rev. D **106**, 024012 (2022). https://doi.org/10.1103/PhysRevD.106.024012
16. C.A. Benavides-Gallego, W.-B. Han, D. Malafarina, B. Ahmedov, A. Abdujabbarov, Phys. Rev. D **104**, 084024 (2021). https://doi.org/10.1103/PhysRevD.104.084024
17. Y.-P. Zhang, S.-W. Wei, Y.-X. Liu, Universe (2020). https://doi.org/10.3390/universe6080103
18. P. Rastall, Phys. Rev. D **6**, 3357 (1972). https://doi.org/10.1103/PhysRevD.6.3357
19. E.J. Copeland, M. Sami, S. Tsujikawa, Int. J. Mod. Phys. D **15**, 1753 (2006). https://doi.org/10.1142/S021827180600942X. arXiv:hep-th/0603057
20. T. Chiba, T. Okabe, M. Yamaguchi, Phys. Rev. D **62**, 023511 (2000). https://doi.org/10.1103/PhysRevD.62.023511
21. C. Schimd, I. Tereno, J.-P. Uzan, Y. Mellier, L. vanWaerbeke, E. Semboloni, H. Hoekstra, L. Fu, A. Riazuelo, Astron. Astrophys. **463**, 405 (2007)
22. V.V. Kiselev, Class. Quantum Gravity **20**, 1187 (2003). https://doi.org/10.1088/0264-9381/20/6/310. arXiv:gr-qc/0210040
23. B. Toshmatov, Z. Stuchlik, B. Ahmedov, Eur. Phys. J. Plus (2015). https://doi.org/10.1140/epjp/i2017-11373-4
24. B. Majeed, M. Jamil, P. Pradhan, Adv. High Energy Phys. **2015**, 124910 (2015). https://doi.org/10.1155/2015/124910. arXiv:1508.04761 [gr-qc]
25. K. Ghaderi, B. Malakolkalami, Astrophys. Space Sci. **361**, 161 (2016). https://doi.org/10.1007/s10509-016-2744-x
26. B. Narzilloev, I. Hussain, A. Abdujabbarov, B. Ahmedov, C. Bambi, Eur. Phys. J. Plus **136**, 1032 (2021). https://doi.org/10.1140/epjp/s13360-021-02039-x. arXiv:2110.01772 [gr-qc]
27. B. Narzilloev, I. Hussain, A. Abdujabbarov, B. Ahmedov, Eur. Phys. J. Plus **137**, 645 (2022). https://doi.org/10.1140/epjp/s13360-022-02872-8. arXiv:2205.11760 [gr-qc]
28. T. Mirzaev, S. Li, B. Narzilloev, I. Hussain, A. Abdujabbarov, B. Ahmedov, Eur. Phys. J. Plus **138**, 47 (2023). https://doi.org/10.1140/epjp/s13360-022-03632-4
29. D.J. Gogoi, Y. Sekhmani, D. Kalita, N.J. Gogoi, J. Bora, Fortschr. Phys. (2023). https://doi.org/10.1002/prop.202300010
30. M. Visser, Phys. Lett. B **782**, 83 (2018)
31. F. Darabi, H. Moradpour, I. Licata, Y. Heydarzade, C. Corda, Eur. Phys. J. C **78**, 25 (2018). https://doi.org/10.1140/epjc/s10052-017-5502-5. arXiv:1712.09307 [gr-qc]
32. T.R. Caramês, M.H. Daouda, J.C. Fabris, A.M. Oliveira, O.F. Piattella, V. Strokov, Eur. Phys. J. C **74**, 3145 (2014)
33. H. Moradpour, Y. Heydarzade, F. Darabi, I.G. Salako, Eur. Phys. J. C **77**, 259 (2017). https://doi.org/10.1140/epjc/s10052-017-4811-z. arXiv:1704.02458 [gr-qc]
34. M.F. Shamir, I. Yaqoot, G. Mustafa, New Astron. **89**, 101624 (2021)
35. Y. Heydarzade, H. Moradpour, F. Darabi, Can. J. Phys. **95**, 1253 (2017). https://doi.org/10.1139/cjp-2017-0254. arXiv:1610.03881 [gr-qc]
36. F.M. da Silva, L.C.N. Santos, C.C. Barros, Class. Quantum Gravity **38**, 165011 (2021). https://doi.org/10.1088/1361-6382/ac129d. arXiv:2010.00086 [astroph. HE]
37. M.R. Shahzad, G. Abbas, Astrophys. Space Sci. **365**, 147 (2020). https://doi.org/10.1007/s10509-020-03861-y
38. G. Abbas, M. Shahzad, Chin. J. Phys. **63**, 1 (2020)
39. M.F. Sakti, A. Suroso, F.P. Zen, Ann. Phys. **413**, 168062 (2020). https://doi.org/10.1016/j.aop.2019.168062

40. R. Kumar, S.G. Ghosh, Eur. Phys. J. C **78**, 1 (2018)
41. M.F.A.R. Sakti, A. Suroso, A. Sulaksono, F.P. Zen, Phys. Dark Univ. **35**, 100974 (2022). https://doi.org/10.1016/j.dark.2022.100974. arXiv:2110.03525 [hep-th]
42. J. Rayimbaev, B. Narzilloev, A. Abdujabbarov, B. Ahmedov, Galaxies (2021). https://doi.org/10.3390/galaxies9040071
43. B. Narzilloev, J. Rayimbaev, A. Abdujabbarov, B. Ahmedov, Galaxies (2021). https://doi.org/10.3390/galaxies9030063
44. B. Narzilloev, B. Ahmedov, Symmetry (2022). https://doi.org/10.3390/sym14091765
45. N. Kurbonov, J. Rayimbaev, M. Alloqulov, M. Zahid, F. Abdulxamidov, A. Abdujabbarov, M. Kurbanova, Eur. Phys. J. C **83**, 506 (2023). https://doi.org/10.1140/epjc/s10052-023-11691-9
46. B. Narzilloev, B. Ahmedov, New Astron. **98**, 101922 (2023). https://doi.org/10.1016/j.newast.2022.101922
47. B. Narzilloev, A. Abdujabbarov, A. Hakimov, Int. J. Mod. Phys. A **37**, 2250144 (2022). https://doi.org/10.1142/S0217751X22501445
48. B. Narzilloev, B. Ahmedov, Symmetry **15**, 293 (2023). https://doi.org/10.3390/sym15020293
49. J. M. Ladino, C. A. Benavides-Gallego, E. Larra.naga, J. Rayimbaev, F. Abdulxamidov (2023). arXiv:2305.15350 [gr-qc]
50. B. Narzilloev, B. Ahmedov, Int. J. Mod. Phys. A **38**, 2350026 (2023). https://doi.org/10.1142/S0217751X23500264
51. J. Rayimbaev, A. Abdujabbarov, F. Abdulkhamidov, V. Khamidov, S. Djumanov, J. Toshov, S. Inoyatov, Eur. Phys. J. C **82**, 1110 (2022). https://doi.org/10.1140/epjc/s10052-022-11080-8
52. J. Rayimbaev, D. Bardiev, F. Abdulxamidov, A. Abdujabbarov, B. Ahmedov, Universe **8**, 549 (2022). https://doi.org/10.3390/universe8100549
53. J. Rayimbaev, S. Shaymatov, F. Abdulxamidov, S. Ahmedov, D. Begmatova, Universe (2023). https://doi.org/10.3390/universe9030135
54. J. Casanellas, P. Pani, I. Lopes, V. Cardoso, Astrophys. J. **745**, 15 (2011)
55. R. Li, J. Wang, Z. Xu, X. Guo, Mon. Not. R. Astron. Soc. **486**, 2407 (2019)
56. Z. Xu, Y. Liao, J. Wang, Int. J. Mod. Phys. A **34**, 1950185 (2019). https://doi.org/10.1142/S0217751X19501859
57. E. Corinaldesi, A. Papapetrou, Proc. R. Soc. Lond. A **209**, 259 (1951). https://doi.org/10.1098/rspa.1951.0201
58. B. Tulzcyjew, Acta Phys. Pol. **18**, 393 (1959)
59. W. BeiglböLock, Commun. Math. Phys. **5**, 106 (1967). https://link.springer.com/article/10.1007/BF01646841
60. B. Tulzcyjew, W. Tulzcyjew, Recent Developments in General Relativity, Pergamon Press, New York (1962)
61. W.G. Dixon, Il Nuovo Cimento **34**, 317 (1964). https://doi.org/10.1007/BF02734579
62. W.G. Dixon, Proc. R. Soc. Lond. A **314**, 499 (1970). https://doi.org/10.1098/rspa.1970.0020
63. W.G. Dixon, Proc. R. Soc. Lond. A **319**, 509 (1970). https://doi.org/10.1098/rspa.1970.0191
64. J. Ehlers, E. Rudolph, Gen. Relat. Gravit. **8**, 197 (1977). https://doi.org/10.1007/BF00763547
65. A.A. Deriglazov, W. Guzmán Ramírez, Adv. Math. Phys (2017). https://doi.org/10.1155/2017/7397159. arXiv:1710.07135 [gr-qc]
66. A.A. Deriglazov, W. Guzmán Ramírez, Phys. Lett. B **779**, 210 (2018). https://doi.org/10.1016/j.physletb.2018.01.063. arXiv:1802.08079 [gr-qc]
67. M. Saijo, K.-I. Maeda, M. Shibata, Y. Mino, Phys. Rev. D **58**, 064005 (1998)
68. C.A. Benavides-Gallego, W.-B. Han, D. Malafarina, B. Ahmedov, A. Abdujabbarov, Phys. Rev. D **104**, 084024 (2021). https://doi.org/10.1103/PhysRevD.104.084024. arXiv:2107.07998 [gr-qc]
69. F. Abdulxamidov, C.A. Benavides-Gallego, W.-B. Han, J. Rayimbaev, A. Abdujabbarov, Phys. Rev. D **106**, 024012 (2022). https://doi.org/10.1103/PhysRevD.106.024012. arXiv:2205.11727 [gr-qc]
70. C. Conde, C. Galvis, E. Larrañaga, Phys. Rev. D **99**, 104059 (2019). https://doi.org/10.1103/PhysRevD.99.104059. arXiv:1905.01323 [gr-qc]
71. B. Toshmatov, D. Malafarina, Phys. Rev. D **100**, 104052 (2019). https://doi.org/10.1103/PhysRevD.100.104052. arXiv:1910.11565 [gr-qc]
72. S.A. Hojman, F.A. Asenjo, Class. Quantum Gravity **30**, 025008 (2013). https://doi.org/10.1088/0264-9381/30/2/025008. arXiv:1203.5008 [physics.gen-ph]